Supplemental Figures and Figure Legends:

Figure S1

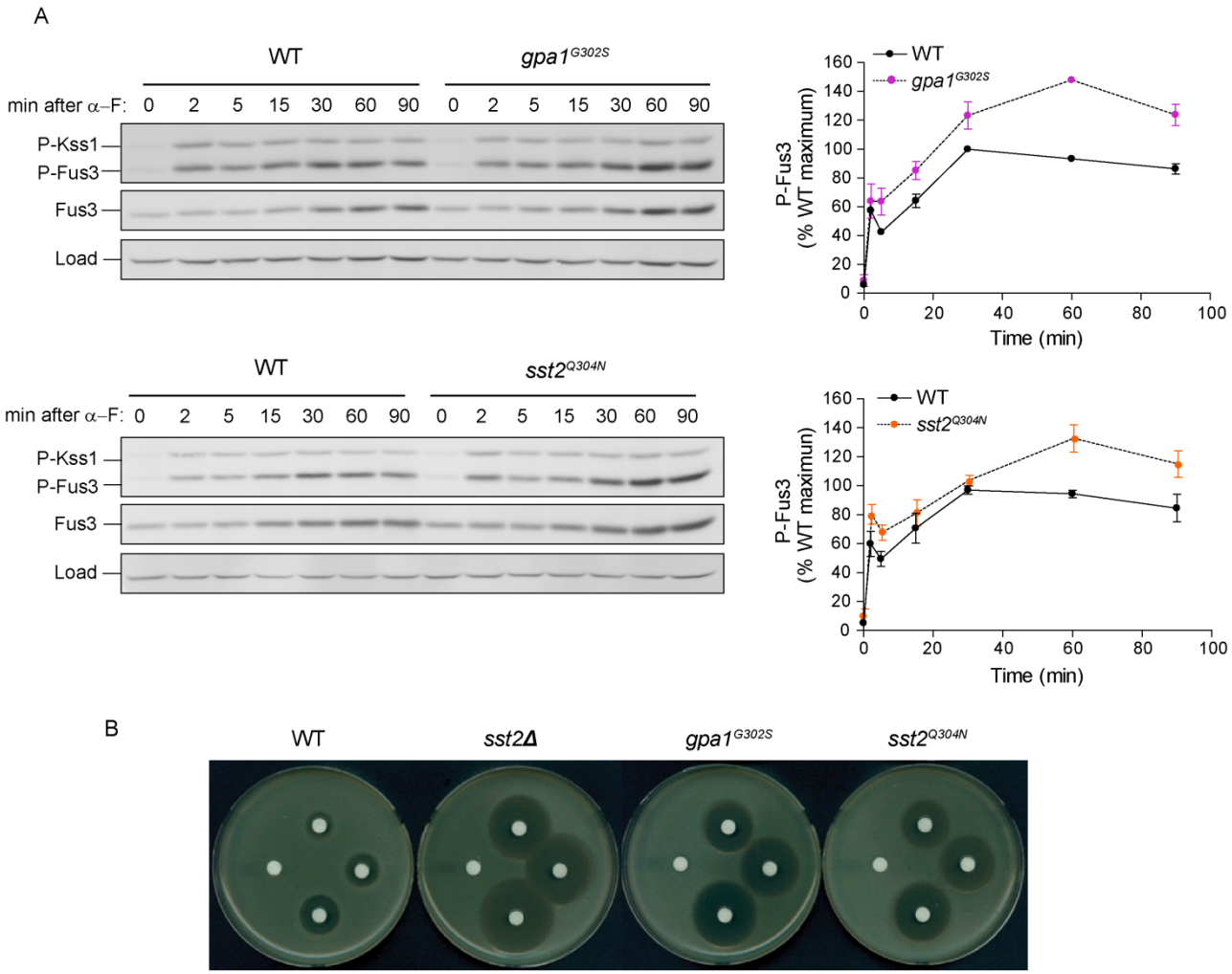

Figure S1: ***gpa1*^{G302S} and *sst2*^{Q304N} are equally sensitive to pheromone**
(A) Time course of phospho-MAPK activation: Wild type cells and mutant strains *gpa1*^{G302S} or *sst2*^{Q304N} were treated with 3 μM α factor and samples collected at the indicated times. MAPK activation was determined by immunoblotting with phospho-p44/42 (P-Fus3, P-Kss1), Fus3 C terminal (Fus3) and G6PDH (Load) antibodies (*left*). Densitometry of P-Fus3 bands normalized to the loading control *(right)*. Results show the mean ± SEM for three individual experiments. **(B)** Halo Assay to measure pheromone induced growth arrest. Disks were spotted with 0, 5, 15 and 50 μg α factor. (Related to Figure 1)

Figure S2

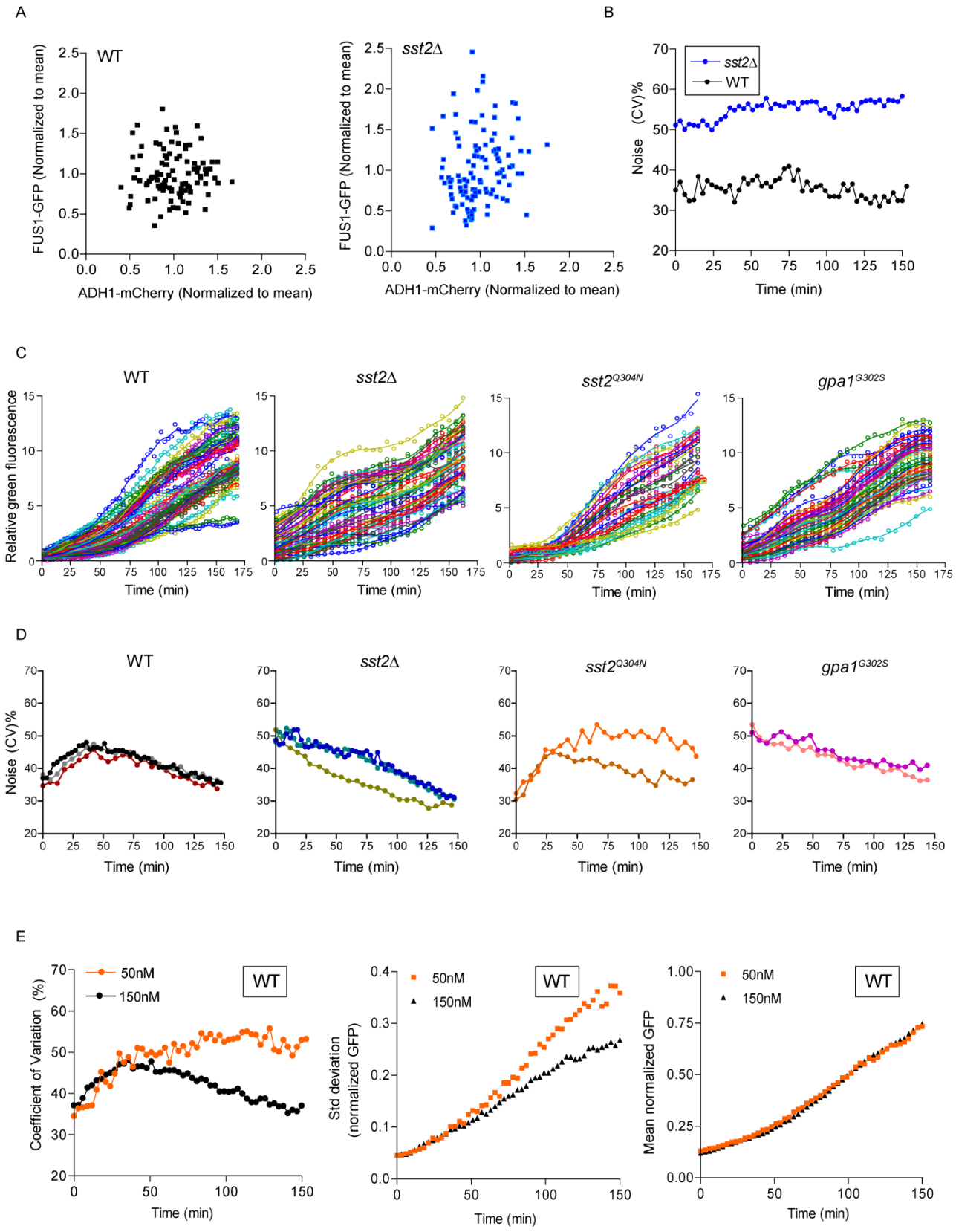
A
WT
FUS1-GFP (Normalized to mean)
ADH1-mCherry (Normalized to mean)
sst2Δ
B
sst2Δ
WT
Noise (CV)%
Time (min)
C
WT
sst2Δ
sst2Q304N
gpa1G302S
Relative green fluorescence
Time (min)
D
Noise (CV)%
Time (min)
E
50nM
150nM
WT
Coefficient of Variation (%)
Std deviation (normalized GFP)
Mean normalized GFP
Time (min)

Figure S2 cont.

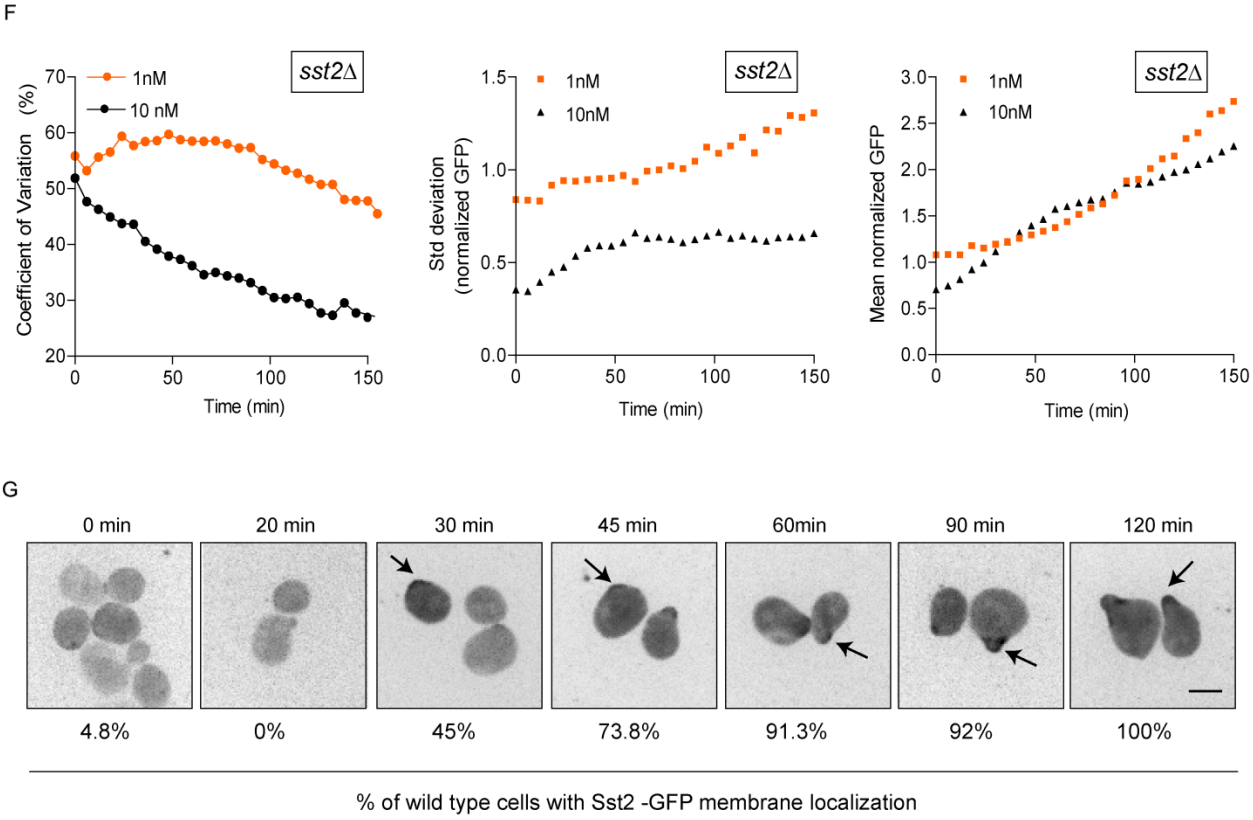

Figure S2: **Noise analysis of pheromone pathway specific gene expression**.
(A) Scatter plots demonstrating pheromone pathway specific (*FUS1*-GFP) and pathway independent (*ADH1*-mCherry) noise in wild type and *sst2*Δ cells. Each point represents the mean fluorescence intensities from one cell.
(B) Change in CV over time in the *absence* of pheromone in wild type and *sst2*Δ cells. Fluorescence and CV measurements were made every 3 min.
(C) Single cell traces of relative GFP (GFP fluorescence/mCherry fluorescence) for wild type, *sst2*Δ, $sst2^{Q304N}$ and $gpa1^{G302S}$ cells over time after treatment with 150 nM α factor. Data represent traces from one experiment with approximately 35-50 cells per condition. To plot the data for each strain on the same Y axis, raw values were normalized such that the mean relative fluorescence at the final time point was assigned a value of 10.
(D) Dynamic changes in CV over time following treatment with 150 nM α factor. Fluorescence and CV measurements were made either every 3 min or every 6 min. Three replicates are shown for wild type and *sst2*Δ cells and two replicates are shown for $sst2^{Q304N}$ and $gpa1^{G302S}$ cells.
(E) Increase in CV in wild type cells upon α factor treatment is sustained when cells are treated with a low dose of pheromone (*left*). Cells were stimulated with either 50 nM (low) or 150 nM (high) α factor and imaged every 3 min. CV was calculated as 'standard deviation of mean GFP' (mCherry normalized) (*middle*) divided by the 'mean GFP' (mCherry normalized) over time

(*right*)**.** Note that the mean (mCherry normalized) GFP is the same at low and high doses of pheromone. The GFP reporter is driven by the α factor-inducible *FUS1* promoter, which is expected to be maximally induced at both high and low concentrations of stimulus.
(F) *sst2*Δ cells exhibit sustained high CV when treated with a low dose of pheromone *(left)*. *sst2*Δ cells were stimulated with either 1 nM (low dose) or 10 nM (high dose) α factor and imaged every 6 min. CV was calculated as standard deviation of mean (mCherry normalized) GFP (*middle*) divided by the mean (mCherry normalized) GFP (*right*). Note that the initial mean fluorescence and standard deviation are different at the two doses owing to differences in the laser power outputs for the microscope on separate days.
(G) Sst2-receptor binding at the membrane is initiated 30 min post pheromone stimulation. Wild type cells expressing GFP-tagged Sst2 were either left untreated or treated with 10 μM (saturating dose) α factor in a shaking culture flask. Samples were collected and imaged on agar pads for Sst2-GFP at the indicated times. Representative GFP (inverted fluorescence) images are shown for each time with the percentage of cells demonstrating Sst2-membrane localization at the bottom of each image. Arrows point to membrane polarized Sst2-GFP. Scale bars, 5 μm. (Related to Figure 2)

Figure S3

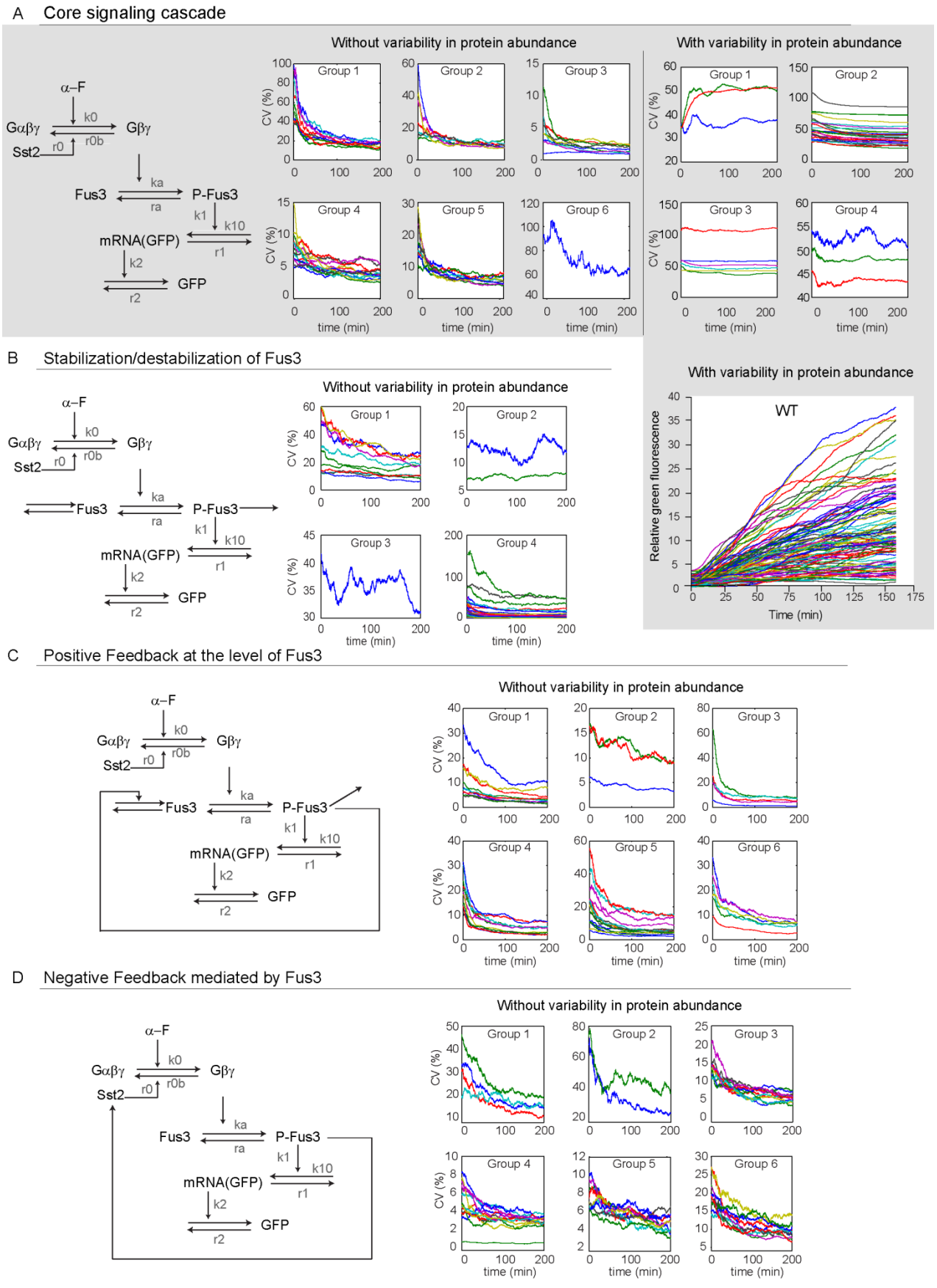
A Core signaling cascade
Without variability in protein abundance
With variability in protein abundance
α–F
Gαβγ
Gβγ
Sst2
k0
r0
r0b
ka
Fus3
P-Fus3
ra
k1
k10
r1
mRNA(GFP)
k2
GFP
r2
Group 1
Group 2
Group 3
Group 4
Group 5
Group 6
CV (%)
time (min)
B Stabilization/destabilization of Fus3
Without variability in protein abundance
With variability in protein abundance
WT
Relative green fluorescence
Time (min)
C Positive Feedback at the level of Fus3
Without variability in protein abundance
D Negative Feedback mediated by Fus3
Without variability in protein abundance

Figure S3: Alternative models tested (left) and corresponding simulations (right) that were unable to capture the dynamic changes in CV of the GFP reporter in wild type cells*$_{\varphi}$.

(A) Model of pathway activation that includes the core signaling cascade: G-αβγ, Fus3, Sst2, mRNA, and GFP *(left)*. Simulations of dynamic changes in CV for wild type cells using the basic activation model (*middle*). Simulations of dynamic changes in CV for wild type cells using the basic activation model *with* variability in protein abundance (*right*). Single cell traces of relative (*FUS1* promoter driven) GFP over time in wild type cells simulated by the basic activation model *with* variability in protein abundance. The initial trajectories generated by the model have shapes that are in agreement with the data shown in Figures 2C and S2C *(bottom right)*.

(B) Model of pathway activation that includes pheromone mediated stabilization or destabilization of Fus3 in the core signaling cascade (*left*). Simulations of dynamic changes in CV for wild type cells with the stabilization/destabilization (of Fus3) model (*right*).

(C) Model of pathway activation that includes positive feedback where activated Fus3 leads to synthesis of more Fus3 in the core signaling cascade (*left*). Simulations of dynamic changes in CV for wild type cells using the positive feedback model (*right*).

(D) Model of pathway activation that includes negative feedback whereby Fus3 increases Sst2 levels, which in turn lowers G protein activity in the core signaling cascade (*left*). Simulations of dynamic changes in CV for wild type cells using the negative feedback model (*right*). (Related to Figure 2)

* All four models incorporate intrinsic fluctuations due to the random nature of biochemical reactions in the cell. Models B, C and D do *not* include any cell-to-cell variability in initial protein levels. None of the models include fluctuations that may be present on long time scales.

$_{\varphi}$ For each of these models 50 parameter sets were chosen from a normal distribution centering on average values derived from the literature. For each model the 50 simulations were grouped using the MATLAB kmeans clustering algorithm with the “distance” option set to “correlation”.

Figure S4

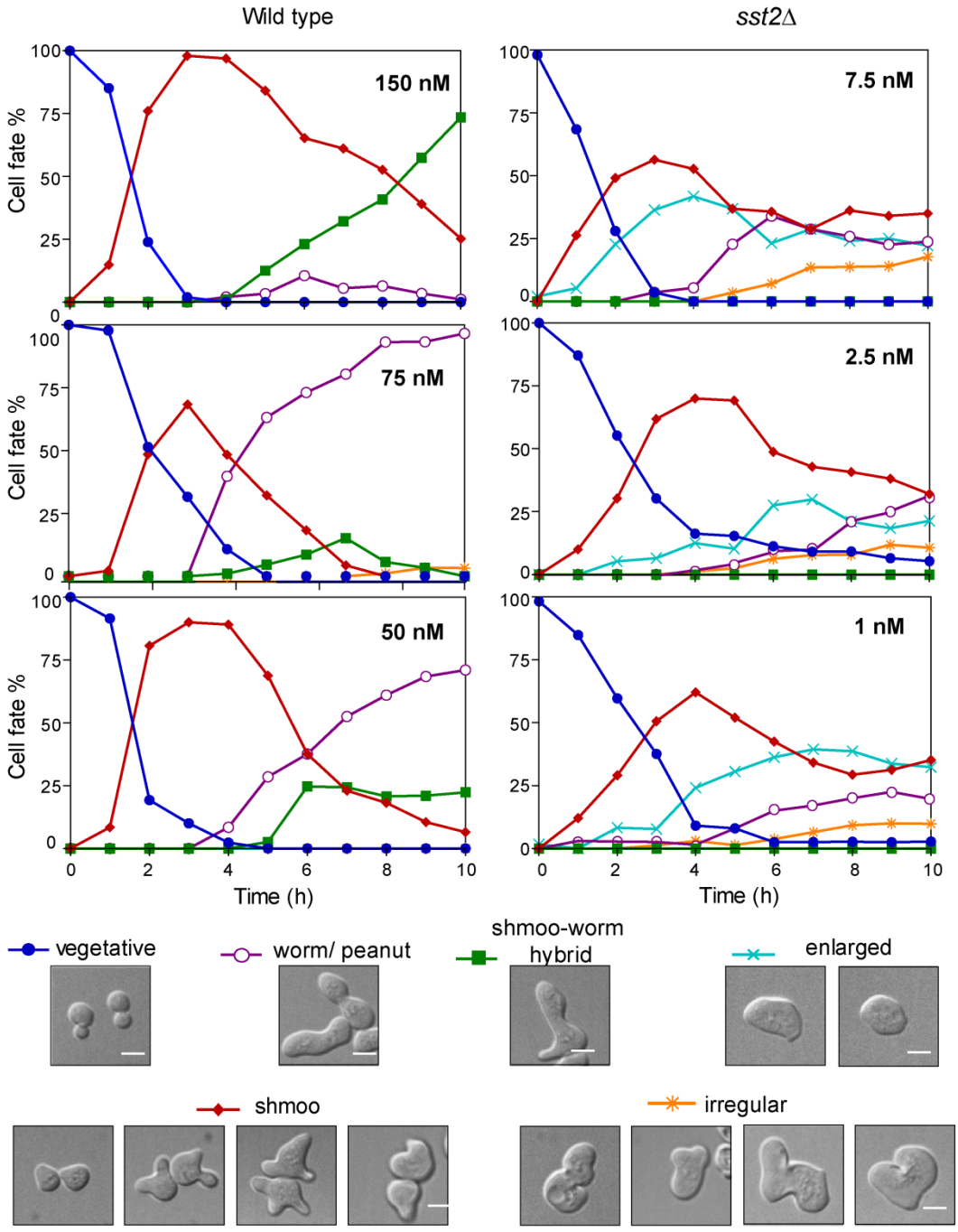

Figure S4: **Sst2 limits heterogeneity in pheromone dependent cell fate (morphology)**. Wild type (*left*) and *sst2*Δ cells (*right*) were treated with the indicated doses of pheromone in a microfluidic chamber and morphological fates of individual cells were tracked every hour up to 10 h. Cells were categorized as follows: (1) vegetative (G1/S/G2/M): budding or small rounded , (2) worm or peanut (elongating): arise from a slight constriction at the polar cap followed by an elongation in that direction over time , (3) shmoo-worm hybrid: arise when cells shmoo once and

subsequently initiate elongation perpendicular to the shmoo, (4) enlarged (circular or ellipse): arise when cells grow in size without polarization, (5) shmoo: (one, two or three well defined constricted projections), and (6) irregular (undefined shapes): arise due to cell expansion and random changes in the direction of polarization over time. Key shows representative images for each morphological class. Each graph contains data from one experiment with at least 100 cells monitored over time. Scale bar, 5 μm. (Related to Figures 3 & 4).

Supplemental Movie S1 Legend:

Movie showing wild type, *sst2*Δ, *sst2*^{Q304N} and *gpa1*^{G302S} cells (merged DIC and Bem1-GFP) responding to saturating dose of α-factor (300 nM) in a microfluidic chamber. Cells were imaged at 5 min intervals for 4 h as described in the experimental procedures. (Related to Figure 4)

Table S1: Table of strains used in this study

Strains	Parent	description
BY4741		*MAT***a** *leu2*Δ *met15*Δ *his3*Δ *ura3*Δ
BY4742		*MAT*α *leu2*Δ *lys2*Δ *his3*Δ *ura3*Δ
sst2Δ	BY4741	*sst2Δ*::KanMX4
gpa1G302S	BY4741	*gpa1*^{G302S}::*URA3*
sst2Q304N	BY4741	*sst2*^{Q304N} integrated and 5 FOA selected
WT FUS1$_p$GFP ADH1$_p$ mCherry	BY4741	*FUS1*$_p$GFP::*HIS3 ADH1*$_p$ mCherry::*URA3*
*sst2*Δ FUS1$_p$GFP ADH1$_p$ mCherry	BY4741	*sst2Δ*::KanMX *FUS1*$_p$GFP::*HIS3* ADH1$_p$mCherry::*URA3*
gpa1^{G302S} FUS1$_p$GFP ADH1$_p$ mCherry	BY4741	*gpa1*^{G302S}::*URA3 FUS1*$_p$GFP::*HIS3 ADH1*$_p$mCherry::*LEU2*
sst2^{Q304N} FUS1$_p$GFP ADH1$_p$ mCherry	BY4741	*FUS1*$_p$GFP::*HIS3 ADH1*$_p$ mCherry::*URA3*
WT Bem1-GFP	BY4741	*BEM1*-GFP::*HIS3*
*sst2*Δ Bem1-GFP	BY4741	*sst2Δ*::KanMX4 Bem1-GFP::*HIS3*
gpa1^{G302S} Bem1-GFP	BY4741	*gpa1*^{G302S}::*URA3* Bem1-GFP::*HIS3*
sst2^{Q304N} Bem1-GFP	BY4741	*sst2*^{Q304N} Bem1-GFP::*HIS3*

Table S2: Table of plasmids used in this study

Name	Description	Source
pRS406 *gpa1*$^{(81-1538)G302S}$	YIp Amp^R *URA3 gpa1*$^{(81-1538)G302S}$	(Lambert et al.)
pRS406 *sst2*^{Q304N}	YIp Amp^R *URA3 sst2*^{Q304N}	This study
pRS423 FUS1-lacZ	2 µm Amp^R *HIS3 FUS1*-lacZ	(Hoffman et al., 2000)
pRS303 FUS1-GFP	YIp Amp^R *HIS3 FUS1*$_p$ GFP	(Siekhaus and Drubin, 2003)
pRS316 ADH1 mCherry	CEN Amp^R *URA3 ADH1*$_P$-*ADH1*$_T$	This study
pRS406 ADH1 mCherry	YIp Amp^R *URA3 ADH1*$_P$-*ADH1*$_T$	This study
pRS405 ADH1 mCherry	YIp Amp^R *LEU2 ADH1*$_P$-*ADH1*$_T$	This study

Table S3: Table of oligonucleotide primer sequences

Name	Sequence 5'-3'
sst2 del (F)	GTTATAGGTT CAATTTGGTA ATTAAAGATA GAGTTGTAAG CGTACGCTGCAGGTCGAC
sst2 del (R)	GTGCAATTGTACCTGAAGATGAGTAAGACTCTCAATGAAA ATCGATGAATTCGAGCTCG
sst2 (F)	ATGC**GGATCC**GTGCTTATAA CTTTAAGAAA AACCAGCGTC
sst2 (R)	ATGC**GGTACC**ATGAATGAATTTGCGTTCAATCCC
sst2-Q304N(F)	TTACAACAAAGGCTATATGG***AAC***TGGATAATGGACTGTACTGAT
sst2-Q304N(R)	ATCAGTACAGTCCATTATCCA***GTT***CCATATAGCCTTTGTTGTAA
mCherryMega (F)	CAAGCTATACCAAGCATACAATCAACTatggtgagcaagggcgaggagg
mCherryMega (R)	GGCGAAGAAGTCCAAAGCTCTGGCGttacttgtacagctcgtccatgccgc
mCherry406 (F)	CCCCC**CTCGAG**GTCGACGGTATCGATAAGCgggaacaaaagctggtaccaagcttagatcc
mCherry406 (R)	CAAAAGCTG**GAGCTC**CACCGCGGTGGCGGCCGCgatccgtgtggaagaacgattacaacagg
ADH1_xhoI (F)	ATG C**CT CGA G**GA AGG TGA GAC GCG CAT AAC CGC
ADH1_SacI (F)	GAC T**GA GCT C**AT CCG TGT GGA AGA ACG ATT ACA ACA GG
Bem1His (F)	TGTCTGAGGAAGAGTTAGAAA
Bem1His (R)	AGTATCTTTGGGCTGCGGTTA

* Red sequence binds pFA6-KanMX. Lower case binds mCherry and upper case binds pRS316ADH1. Restriction enzyme sites are indicated in bold letters.

Table S4: Model parameter values and reactions

Parameter Name	Description	Best Value	Mean in random search	Reaction
k0	Dissociation of Gβγ from Gα: Pheromone dependent input	3 e-4 1/sec	2e-3 1/sec	Gαβγ -> Gβγ + Gα
k1	Fus3 dependent transcription	8.2e-6 1/sec	2 e-05 1/sec	P-Fus3 -> P-Fus3 + mRNA
k10	Fus3 independent transcription	0.0013 molec/sec	2e-3 molec/sec	-> mRNA
k2	Translation rate	0.004 1/sec	1.5e-3 1/sec	mRNA -> mRNA + GFP
ka	Activation/phosphorylation rate of Fus3. Dependent on Gβγ	7.6e-4 (1/sec*molec)	5e-3 1/(sec*molec)	Fus3 + Gβγ -> P-Fus3 + Gβγ
r0	Sst2 dependent association of Gα, Gβγ	4 (1/sec*molec^2)	5 (1/sec*molec^2)	Sst2 + Gβγ + Gα -> Sst2 + Gαβγ
r0b	Sst2 independent association of Gα, Gβγ	0.004 (1/sec*molec)	.005 1/(sec*molecule)	Gβγ + Gα -> Gαβγ
r1	Degradation rate of mRNA	0.0017 1/sec	0.0017 1/sec	mRNA
r2	Degradation rate of GFP	1.6e-04 1/sec	1.6e-04 1/sec	GFP ->
ra	Deactivation /de-phosphorylation rate of P-Fus3	0.11/(sec)	0.11/(sec)	P-Fus3 -> Fus3
Total Fus3		8000 molec/cell	8000 molec/cell	*Source: (Ghaemmaghami et al., 2003)
Total G protein		8000 molec/cell	8000 molec/cell	

Supplemental Experimental Procedures

Plasmid Construction: The pRS406 ADH1-mCherry and pRS405 ADH1-mCherry integrating vectors were constructed in two steps, both employing mega-primer cloning (Unger et al., 2010). First, mCherry was PCR amplified using pRS405 STE2-mCherry as the template and the following primers: mCherryMega (F) and mCherryMega (R). The primers introduced sequences at the N and C termini of mCherry complementary to the *ADH1* promoter and *ADH1* terminator sequences in pRS316 ADH1. Subsequently, *ADH1*p-mCherry-$ADH1_t$ was PCR amplified from pRS316 ADH1-mCherry with primers [ADH1_XhoI (F) and ADH1_SacI (R)] that also introduced terminal XhoI/SacI sites and overhangs that direct $ADH1_p$-mCherry-$ADH1_t$ into the MCS of pRS406 and pRS405. pRS406 $sst2^{Q304N}$ was made by PCR amplification of *SST2* +/- 500 bp from the gDNA of wild type cells using primers sst2 (F) and sst2 (R) that introduced BamHI and KpnI sites for directional cloning into pRS406. Single point mutation of $sst2^{Q304N}$ was constructed by QuikChange (Stratagene) mutagenesis using primer sst2-Q304N-F and its complement.

Strain Construction: The *sst2Δ* (BY4741 *sst2Δ*::KanMX4) strain from Research Genetics did not produce a consistent phenotype. It was remade by PCR amplification of the KanMX cassette of pFA6KanMX and transformation into wild type BY4741 (Wach et al., 1994). The GAP insensitive Gpa1 strain $(gpa1^{G302S})$ was constructed as described earlier (Lambert et al.). The receptor uncoupling strain ($sst2^{Q304N}$) was constructed by transformation of pRS406 $sst2^{Q304N}$ (linearized by AscI) followed by pop-out of the wild type allele on 5-Fuoroorotic acid-containing medium. All constructs were verified by nucleotide sequence analysis.

Generating dual reporter strains with pathway specific GFP and reference mCherry
Pathway specific GFP reporter was integrated at the *FUS1* promoter by transformation of pRS303 FUS1-GFP linearized by digestion with XcmI. Positive clones with one *FUS1*-GFP integration were selected by growth on SCD–His medium and transformed with PacI-digested pRS406 ADH1-mCherry that integrated at the *ADH1* promoter. Transformants selected on

medium lacking uracil were deemed positive only if they had a single integration as assessed by mCherry fluorescence intensity. This process was applied to all other strains except *gpa1*^{G302S} which was transformed with pRS405 ADH1-mCherry.

Generating reporter strains to monitor polarization. BEM1-GFP was PCR amplified from the GFP-tagged library strain (Huh et al., 2003). Briefly, genomic DNA was isolated and used as a template for PCR with primers [Bem1His (F) and Bem1His (R)] that amplified a portion of the C' of *BEM1* along with GFP and *HIS3*. The PCR product was transformed in wild type, *sst2Δ, gpa1*^{G302S} *and sst2*^{Q304N} cells, and selected on medium lacking histidine.

Intracellular variability calculation: We calculated the trend-line for the single cell GFP intensity traces over time, using the MATLAB "smooth" function, with a span of 7 time points and a "lowess" fit. The absolute value of the difference of the actual data from the smoothed line was divided by the value of the smoothed line to determine the coefficient of variation at each time point. There was little variation in intrinsic noise over time, so the coefficients of variation for all time points were averaged for all cells to determine the average coefficient of variation for each strain.

Morphology analysis at uniform pheromone: Log phase cells were loaded onto a microfluidic chamber at low density. Cells were stimulated with saturating pheromone (150 nM for wild type cells and 7.5 nM for *sst2*Δ), intermediate pheromone (75 nM for wild type cells and 2.5 nM for *sst2*Δ) or low-intermediate pheromone (50 nM for wild type cells and 1 nM for *sst2*Δ). DIC images were taken every 6 min for 10 h to track changes in cell morphology. Morphological cataloging was done by manually binning cells in predefined classes using ImageJ to visualize cells over time.

Image Analysis for cell polarization during gradient tracking: Images were analyzed with FIJI (Fiji Is Just Imagej) for cell tracking and polar plot generation from live cell microscopy. The GFP channel was registered based on the DIC channel using "descriptor based series registration." The Bem1-GFP images were then thresholded to select just the polar cap. The

"Analyze Particles" function was used to obtain the centroid of each polar cap throughout the time course. Using MATLAB, the polar caps were assigned to their respective cells by starting with the last time point, and comparing all of the centroids to the centroids of the previous time point. The distances of each object were calculated from the previous time point, and the object that was closest in the preceding time point was assigned to the same cell as in the current time point. This pairwise comparison of polar caps by time points was iterated through the entire time series. The polar plots were generated by time averaging the x,y positions of the polar caps over 10 time points (50 min). The starting point for each cell was set to zero, and the x,y positions were converted to polar coordinates and plotted using the MATLAB polar plot function. Measurements for final angles of orientation during gradient tracking were calculated from the difference in x and y positions between two points (the final time averaged position and the position 1 h earlier) using the MATLAB atan2 function. Persistence was calculated as the ratio of the direct distance between the first and last x,y position and the total distance traveled, defined as the sum of the distances between each consecutive x,y position.

Shmoo Angle Determination: In order to determine the orientation of the polar cap during mating projection formation, cell masks were created using FIJI to define cells, and were then analyzed by custom MATLAB script. Briefly, for each time point and in each cell two regions of interest (ROI) were defined by thresholding at the 95th percentile and 75th percentile of Bem1 intensity. The angle of orientation was determined using the angle defined by the centroid of the 95% threshold ROI and the centroid of the 75% threshold ROI. Each cell was then normalized to an average of zero by subtracting the average angle of orientation of the cell from each data point. A Gaussian was fit to each distribution, and the constant c was used as the standard deviation of the distribution, where the Gaussian is written $f(x) = ae^{-\frac{(x-b)^2}{2c^2}}$.

Stochastic model of change in CV over time: Ordinarily the variability of protein expression, measured by the coefficient of variation (CV), is expected to decrease as the

average protein concentration increases (Kaern et al., 2005). The fact that the CV of pheromone-dependent gene expression increases transiently following pheromone stimulation (at the same time that the average GFP concentration increases) is unexpected. Further, deleting the negative regulator, Sst2, changes the dynamic behavior of the noise: basal noise increases and pheromone induction only results in a decrease in CV over time. To help elucidate the mechanism of the increase in CV over time in wild type cells, and the decrease in CV over time in *sst2*Δ cells, we built several stochastic models (Figure S3). All the models are variants of the core signaling cascade (Model A, Figure S3). In the core model (Model A), α-factor promotes the release of Gβγ. Free Gβγ increases the rate at which Fus3 is activated by phosphorylation, which in turn promotes transcription and eventually translation of the GFP reporter. Additionally, the model assumes a basal level of transcription and translation that is independent of Fus3 activity. Sst2 promotes the re-association of Gβγ to Gα, shutting off the pathway. The variants of the core signaling cascade that also were investigated include: i) stabilization/destabilization of Fus3 following activation (Model B, Figure S3), ii) positive feedback via induction of Fus3 (Model C, Figure S3) and iii) negative feedback via induction of Sst2 (Model D, Figure S3). In all the models, cell-to-cell variability of protein concentrations is assumed to be negligible.

For each model, 50 parameter sets were chosen from a normal distribution centered on average values derived from the literature (Ghaemmaghami et al., 2003). For each parameter set 50 realizations were simulated and used to compute the CV as a function of time. The time series for the CVs were grouped using the MATLAB kmeans clustering algorithm with the "distance" option set to "correlation" (Figure S3, middle panels). None of the models on their own were able to capture the initial increase in the CV over time that was observed experimentally in wild type cells (Fig. 2E). These results suggest that an alternative mechanism involving extrinsic noise underlies this unexpected behavior.

To investigate this possibility, we went back to the core signaling cascade (Model A, Figure S3) and included cell-to-cell variations in the abundance of Fus3 and G protein. In this case for every parameter set, the total level of the MAPK Fus3 and G protein are randomly chosen, from a normal distribution, for each simulation with the variance being 30%. The mean of the distribution is taken from reported values of the protein concentrations (Ghaemmaghami et al., 2003). To find a parameter set that best describe our data, we performed a parameter search choosing from a multivariate normal distribution with mean values chosen from the literature, as before. The CVs for this model were clustered using the same procedure as described above (Figure S3A, right panel). Only 3 of the 50 randomly chosen parameter sets qualitatively agree with the data. The successful parameter sets had several key features in common that are required for the model to reproduce the experimental data: basal activity of pathway components needs to be low, the relative contribution of Fus3-*in*dependent gene expression on total noise after pathway activation needs to be low, and pathway activation following pheromone stimulation should be high. If any of these conditions are not met the CV will not increase over time. Therefore it is easy to see why a random search of parameter space did not produce many parameter sets that reproduced the experimental data. For the best performing parameter set cell-to-cell variability in the abundance of signaling proteins can account for the experimentally observed increase in the CV. Finally, we set the abundance of Sst2 to zero and verified that this model reproduced the decrease in CV over time seen in this strain. The representative results shown in Figure 2F were generated using the parameter values given in Table S4.

Supplemental References

Ghaemmaghami, S., Huh, W. K., Bower, K., Howson, R. W., Belle, A., Dephoure, N., O'Shea, E. K., and Weissman, J. S. (2003). Global analysis of protein expression in yeast. Nature *425*, 737-741.

Hoffman, G. A., Garrison, T. R., and Dohlman, H. G. (2000). Endoproteolytic processing of Sst2, a multidomain regulator of G protein signaling in yeast. J Biol Chem *275*, 37533-37541.

Huh, W. K., Falvo, J. V., Gerke, L. C., Carroll, A. S., Howson, R. W., Weissman, J. S., and O'Shea, E. K. (2003). Global analysis of protein localization in budding yeast. Nature *425*, 686-691.

Kaern, M., Elston, T. C., Blake, W. J., and Collins, J. J. (2005). Stochasticity in gene expression: from theories to phenotypes. Nat Rev Genet *6*, 451-464.

Lambert, N. A., Johnston, C. A., Cappell, S. D., Kuravi, S., Kimple, A. J., Willard, F. S., and Siderovski, D. P. Regulators of G-protein signaling accelerate GPCR signaling kinetics and govern sensitivity solely by accelerating GTPase activity. Proc Natl Acad Sci U S A *107*, 7066-7071.

Siekhaus, D. E., and Drubin, D. G. (2003). Spontaneous receptor-independent heterotrimeric G-protein signalling in an RGS mutant. Nat Cell Biol *5*, 231-235.

Unger, T., Jacobovitch, Y., Dantes, A., Bernheim, R., and Peleg, Y. (2010). Applications of the Restriction Free (RF) cloning procedure for molecular manipulations and protein expression. Journal of structural biology *172*, 34-44.

Wach, A., Brachat, A., Pohlmann, R., and Philippsen, P. (1994). New heterologous modules for classical or PCR-based gene disruptions in Saccharomyces cerevisiae. Yeast *10*, 1793-1808.